International Journal of Impact Engineering 79 (2015) 22–31

Contents lists available at ScienceDirect

International Journal of Impact Engineering

journal homepage: www.elsevier.com/locate/ijimpeng

Dynamic shear punch behavior of tungsten fiber reinforced Zr-based bulk metallic glass matrix composites

J.H. Chen [a], Y. Chen [a], M.Q. Jiang [a], X.W. Chen [b], H.M. Fu [c], H.F. Zhang [c], L.H. Dai [a, d, *]

[a] State Key Laboratory of Nonlinear Mechanics, Institute of Mechanics, Chinese Academy of Sciences, Beijing 100190, China
[b] Institute of Systems Engineering, CAEP, Sichuan 621999, China
[c] Shenyang National Laboratory for Materials Science, Institute of Metal Research, Chinese Academy of Sciences, Shenyang 110016, China
[d] State Key Laboratory of Explosion Science and Technology, Beijing Institute of Technology, Beijing 100081, China

ARTICLE INFO

Article history:
Available online 15 July 2014

Keywords:
Dynamic loading
Shear punch
Bulk metallic glass composite
Tungsten fiber
Failure mode

ABSTRACT

Dynamic shear punch tests were carried out on the tungsten fiber reinforced Zr-based bulk metallic glass composites. The experimental results show that with the increasing fiber volume fraction, the failure mode of the composites switches from shear to tensile fracture. A new failure criterion, based on the Tsai-Hill criterion and the unified failure criterion for bulk metallic glasses, is proposed to characterize fracture behavior of this bulk metallic glass composite. It is found that the shear-to-normal strength ratio α controls the transition of failure mode of this metallic glass composite. The underlying mechanism of the transition of failure mode is discussed as well.

1. Introduction

Bulk metallic glasses (BMGs) have many excellent mechanical and physical properties due to their unique microstructure [1–4]. However, the poor plasticity and subsequent premature fracture, which are attributed to the highly-localized shear deformation, still limit their applications [5–11]. The development of BMG composite is an effective way to surmount this problem [12–16]. The existence of crystalline phase in the BMG composite can promote the multiplication of shear bands, which can accommodate more plastic strain and contribute to macroscopic plasticity. Since it was first fabricated by Dandliker et al. [17], the tungsten fiber/BMG matrix composite, had attracted large interest during the past years [18–21]. This composite exhibits considerable plasticity under compression [18–21]. Furthermore, due to its unique "self-sharpening" behavior in high velocity penetration, the tungsten fiber/BMG matrix composite has approximately a 10–20% improvement in penetrator efficiency over the traditional tungsten heavy alloys [22,23]. This mechanical property promotes the application of the composite to defense field. Though the mechanism of this "self-sharpening" behavior remains elusive, previous studies suggest that this phenomenon may relate to the transverse shear property of this composite [21–25]. Actually, the tungsten fiber/BMG matrix composite is a complex system that contains both crystalline tungsten fiber and amorphous matrix. The resistance of these two phases to shear should be very different due to their intrinsic differences in microstructure [26,27]. Therefore, it can be naturally speculated on that, under transverse shear loading, the global mechanical behavior of the composite should depend on the relative volume ratio of its component phases. However, up to now, no researches have been carried out to study the transverse shear failure behavior of this composite.

In this study, using the split Hopkinson pressure bar (SHPB), dynamic transverse shear punch tests were performed on a tungsten fiber reinforced Zr-based BMG composite with different fiber volume fractions. A new failure criterion is proposed for this composite. The underlying fracture mechanism of this composite under transverse shear loading is revealed. Our present results shed new insights into the deformation and fracture mechanism of the BMG composite.

2. Experimental

2.1. Sample preparation

The chemical composition of the composite matrix is $Zr_{41.25}Ti_{13.75}Ni_{10}Cu_{12.5}Be_{22.5}$ (Vit1). This BMG has excellent amorphous forming ability. Crystalline tungsten fiber with a nominal diameter of 300 μm was used as the reinforcement of the

* Corresponding author. State Key Laboratory of Nonlinear Mechanics, Institute of Mechanics, Chinese Academy of Sciences, Beijing 100190, China. Tel.: +86 10 82543958; fax: +86 10 82543977.
E-mail address: lhdai@lnm.imech.ac.cn (L.H. Dai).

http://dx.doi.org/10.1016/j.ijimpeng.2014.07.006
0734-743X/

composite. The tungsten fiber/Vit1 BMG composite was prepared by the method of pressure infiltration. Details of the casting process are described elsewhere [17,19]. Cross section of the tungsten fiber/Vit1 BMG composite is observed by a scanning electron microscope (SEM), which is shown in Fig. 1. The tungsten fibers are homogeneously distributed in the continuous amorphous matrix. Rectangular specimens, in which tungsten fibers are unidirectionally aligned in the direction parallel to the longer sides, are used in the present study. Vit1 BMG and its tungsten fiber composites with tungsten fiber volume fraction of 40%, 60%, 80% are cut into a dimension of 2.1 × 2.1 × 10 mm by wire electrical discharge machining. The surfaces of the specimens are mechanically polished before testing. The specimens are shown in the insert of Fig. 1. At least six specimens of each fiber volume fraction were tested.

2.2. Shear punch testing

Shear punch testing was performed using a specially designed fixture in an SHPB apparatus. The schematic illustration of shear punch fixture and its geometrical configuration are shown in Fig. 2(b). The fibers in the specimen are unidirectionally aligned in the direction perpendicular to the loading direction. During the test, this fixture is sandwiched between the incident and transmitted bars, as shown in Fig. 2(c). A gas gun lunches the striker bar to impact the incident bar. At the moment of impact, the elastic wave generated in the incident bar compresses the punch. Then the specimen under the punch is displaced into the tubular die. This produces a shear zone in the connection area between the punch and the die, as marked by red area in Fig. 2(b). The shear stress and shear strain can be calculated according to the incident wave $\varepsilon_i(t)$, the reflected wave $\varepsilon_r(t)$, measured by the gauges on the input bar, and the transmitted wave $\varepsilon_t(t)$, measured by the gages on the output bar as follows [28,29]

$$\tau = \frac{EA_1[\varepsilon_i(t) + \varepsilon_r(t) + \varepsilon_t(t)]}{4HD} \quad (1)$$

$$\gamma = \frac{C_0}{B}\int_0^t [\varepsilon_i(t) - \varepsilon_r(t) - \varepsilon_t(t)]\mathrm{d}t \quad (2)$$

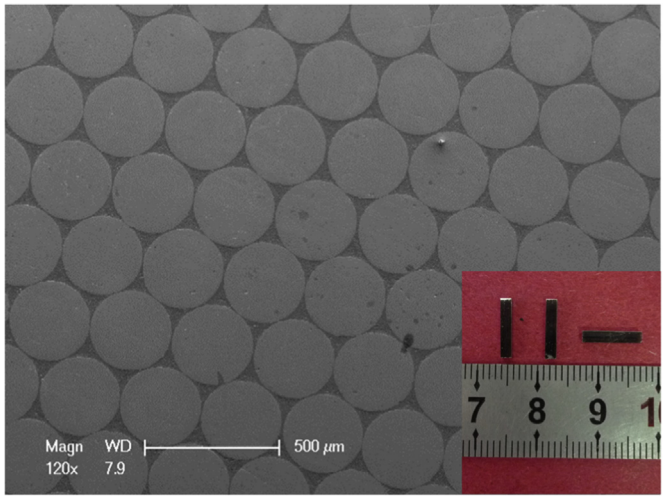

Fig. 1. SEM cross-sectional image of the tungsten fiber/Vit1 BMG matrix composite. Insert shows the polished specimens.

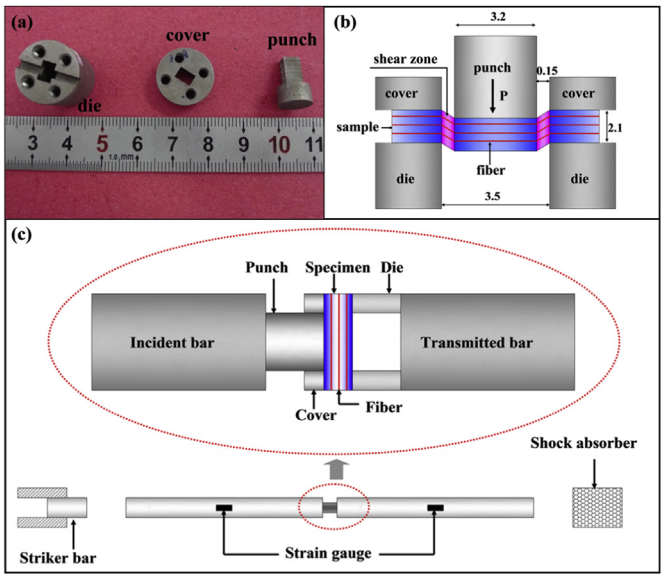

Fig. 2. (a) Photographs of the die, cover and punch. (b) The shear punch setup and its geometrical configuration (dimension in mm). (c) Schematic for the dynamic shear punch test.

where C_0, E and A_1 are elastic wave velocity, elastic modulus and cross section area of the pressure bar, respectively. H is the specimen thickness, and D is specimen width. They are both 2.1 mm in this study. B is the die-punch clearance, which has the value of 0.15 mm (Fig. 2(b)).

After testing, an FEI Sirion high-resolution SEM was used to characterize the fracture morphologies of all specimens.

3. Experimental results

3.1. Mechanical behavior

The typical shear stress versus shear strain curves of tested specimens under dynamic shear punch loading are shown in Fig. 3. It can be seen from Fig. 3 that, for both Vit1 BMG matrix and its composites, the materials exhibit a quasi-brittle behavior and little macroscopic plasticity. After the peak stress, i.e., fracture stress, the stress drops rapidly. Fig. 4 shows that the shear fracture stress of the tested specimens varies with the tungsten fiber volume fraction (V_f). When V_f increases from 0% to 80%, the corresponding fracture stress changes slightly from 1.10 GPa to 1.46 GPa.

3.2. Fracture morphologies

Since the failure mode can be distinguished by the fracture morphologies, all the tested specimens are carefully examined by SEM. Figs.5–8 present the SEM micrographs of the punch-deformed specimens of the composite with V_f of 0% (Vit1 BMG matrix), 40%, 60% and 80%, respectively. From these observations, it can be seen clearly that the failure mode shifts from shear to tensile with the increasing fiber volume fraction. The detailed discussions of each kind of specimen are shown in the following paragraphs.

The typical fracture morphologies of specimen with 0% V_f (Vit1 BMG matrix) are shown in Fig. 5. Fig. 5(a) shows side view of the fractured specimen. It can be seen that the fracture surface is smooth. Fig. 5(c)–(f) shows the details corresponding to the four marked areas which list from upper to the bottom in Fig. 5(b), respectively. As shown in Fig. 5(c), there exists a fracture slip zone at the edge of fracture surface. This zone has the size of about

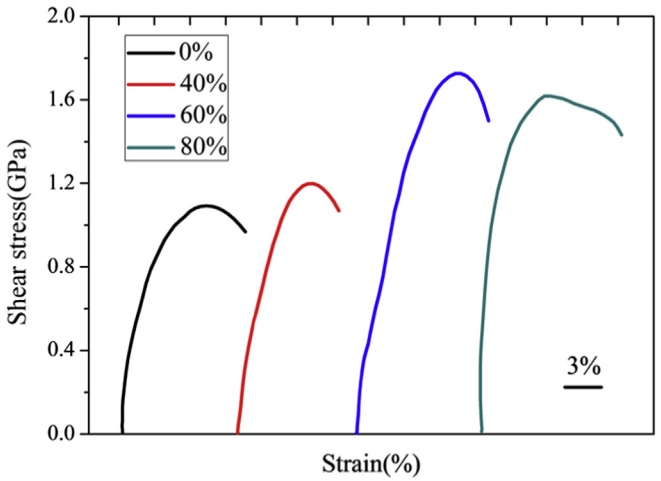

Fig. 3. Typical shear stress–strain curves of the composite with 0% (Vit1 BMG), 40%, 60% and 80% tungsten fiber volume fraction.

30 μm. Typical cell-like vein patterns can be observed in the followed fracture surface, as shown in Fig. 5(d) and (e). Melted region can also be observed, which was presented in Fig. 5(f). These cell-like vein pattern and melted region are the typical fracture morphologies of BMG under dynamic shear loading [30,31]. So, it is reasonable to conclude that in the present shear punch condition, the 0% V_f (Vit1 BMG matrix) specimen fractures by shear.

Fig. 6 shows the specimen of the composite with 40% V_f Compared with the 0% V_f (Vit1 BMG matrix), the fracture surface is rougher, as shown by the side view of the specimen (Fig. 6(a)). Fig. 6(b)–(f) show the fracture morphologies of this specimen. The tungsten fiber/BMG matrix interface is shown in Fig. 6(c). Cell-like vein pattern can be observed for the BMG matrix, indicating a shear fracture mode. Fig. 6(d) is a magnified SEM picture corresponding to the area marked in Fig. 6(c).Tungsten fiber exhibits a stair-step-like pattern. According to the study by Leber et al. [32], this is the typical morphology of tungsten fiber under shear loading. Fig. 6(e) and Fig. 6(f) show another region of the fracture surface. Fig. 6(f) gives details corresponding to the area marked in Fig. 6(e). Typical cleavage fracture morphology can be observed on the tungsten fiber, showing a fracture mode of tension [32]. From the morphologies observed, it can be seen that both the shear and tensile fracture exist in 40% V_f composite. This composite shows a mixed failure mode.

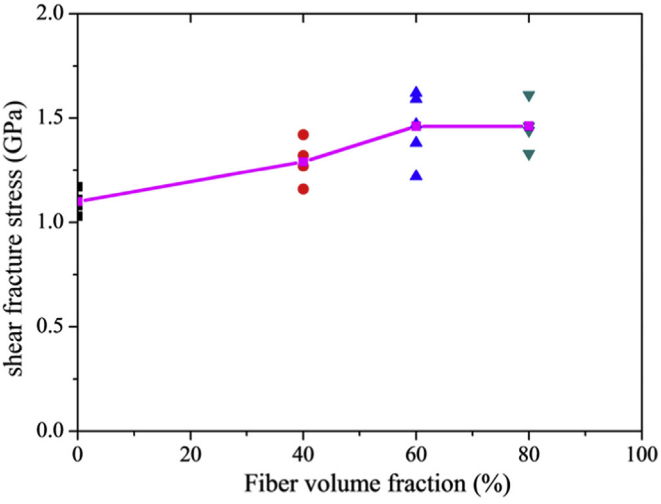

Fig. 4. Shear fracture stress of the composite varies with tungsten fiber volume fraction.

Specimen of composite with 60% V_f is shown in Fig. 7. As can be seen from Fig. 7(a), the fracture surface is rough, similar to the composite with 40% V_f. Many micro-cracks can be observed on the fracture surface, as shown by the arrows in Fig. 7(b). Fig. 7(d) presents the details of BMG matrix corresponding to the area marked in Fig. 7(c). In contrast to the cell-like vein pattern, equiaxial-shaped dimple-like pattern is observed. This indicates a tensile fracture of the BMG matrix [33,34]. Fig. 7(f) is a magnified picture corresponding to the marked area in Fig. 7(e). Tungsten fiber shows the fibrous fracture morphology. This morphology results from tensile fracture [32]. Fig. 7 indicates that the composite with 60% V_f fails in tensile fracture.

Fig. 8 gives the fracture behavior of the specimen with 80% V_f. The river-like vein pattern is observed on the BMG matrix, as shown in Fig. 8(d). According to the studies by Jiang et al. [35] and Raghavan et al. [36], such vein pattern is the typical morphology in the crack initiation zone of BMG which fractures by tension. The fibrous fracture morphology of the tungsten fiber is shown in Fig. 8(f). This indicates that the tensile fracture occurs. Similar to the composite with 60% V_f, the composite with 80% V_f also facture by tensile mode.

From the aforementioned observations of the fracture morphologies of all tested specimens, it can be concluded that the failure mode of the tungsten fiber/BMG composite changes from shear fracture to tensile fracture with the increasing fiber volume fraction. The mechanism for this failure mode transition will be discussed in the next section.

4. Discussion

4.1. Analysis of stress

Firstly, we will analyze the stress state in the shear zone. In the present shear punch test, there is stress concentration in the top and bottom regions of the specimen, where the punch and die are in contact, respectively. This stress concentration will affect the process of fracture. Li and Jones [37,38] studied the response of beam subjected to transverse dynamic impact. According to their experimental observations and finite-element numerical simulations [38], the failure of the beam, either a tensile failure or a shear fracture, is initiated from these stress concentration regions. For our case, supposing the factors of stress concentration is K. Then the shear stress and tensile stress in the stress concentration regions may be expressed as $K\tau$ and $K\sigma$, respectively. Here, τ and σ are shear stress and tensile stress in these regions when stress concentration is not considered. Then, we can get that $K\tau/K\sigma = \tau/\sigma$. From this, it can be seen that the shear-to-normal stress factor in the region of stress concentration may be the same as the region in which stress concentration is not considered. For simplification, the shear-to-normal stress factor is calculated under the condition that the stress concentration is not considered in the shear zone in the shear punch test. Thus, the shear punch test can be simplified to that a beam is loaded under the uniformly distributed load, as shown in Fig. 9(a).

For a simple beam under a uniform load, there exists both shear and normal stress in the cross section of the beam. According to the results from the theory of elasticity [39], the distribution of shearing stresses in a transverse section of a rectangular beam is parabolic. The maxima shearing stresses are in the neutral axis, while the shearing stresses are zero at the top and bottom of the cross section. However, as shown by Hankin et al. [40], the true multiaxial, non-uniform stress state in the shear zone is a relatively

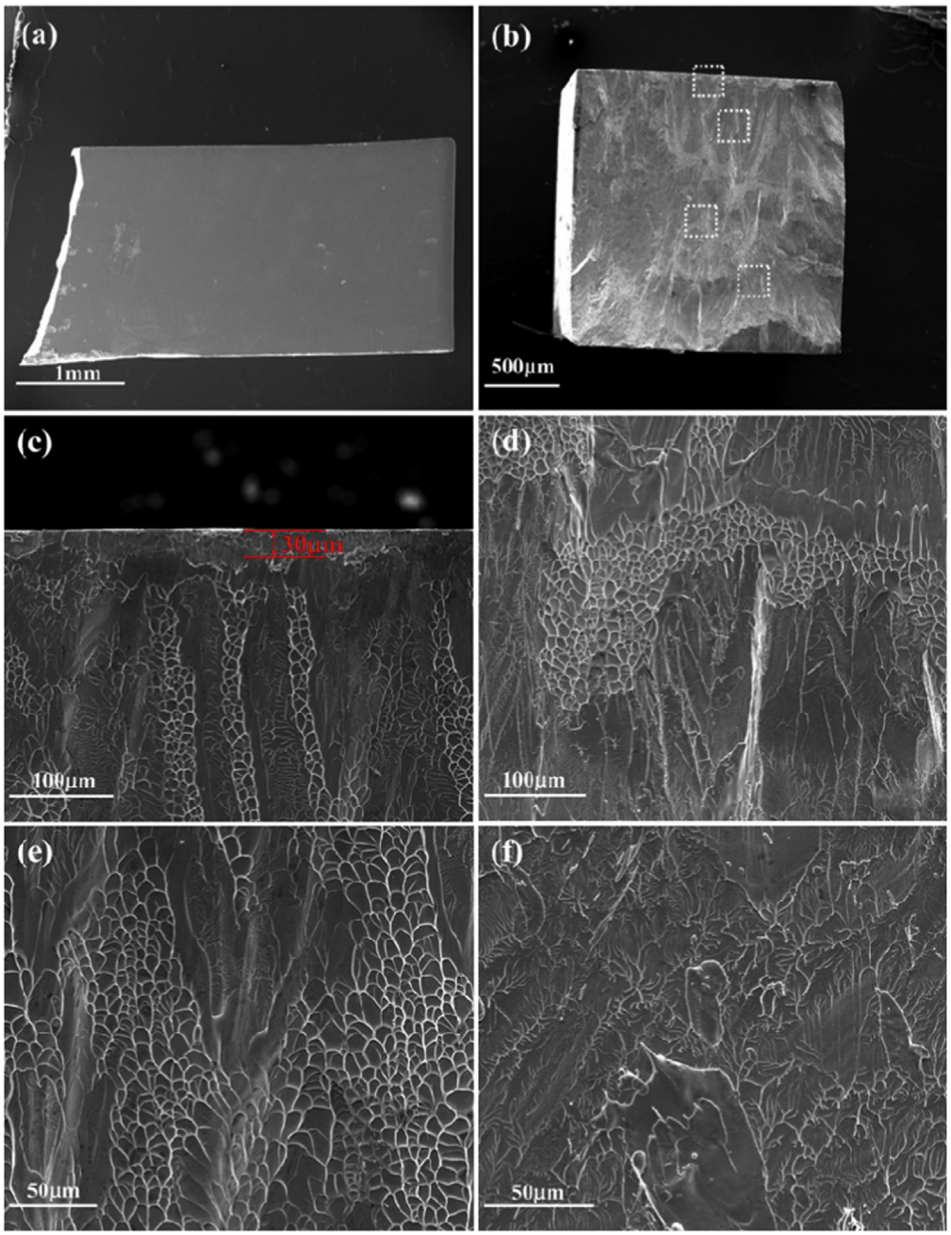

Fig. 5. Fracture characteristics of specimen with 0% V_f (Vit1 BMG) under shear punch test. (a) Side-view of the fractured specimen. (c)–(f) Details corresponding to the areas marked in (b).

uniform shear combined with normal stress. Thus, for the shear punch test, it is reasonable to appropriately define the shear stress as

$$\tau = \frac{F}{A} = \frac{qD_{\text{die}}}{2DH} \tag{3}$$

where F is the shear force and A is the area of the cross section. q is the distributed load, and D_{die} is the diameter of the die. Actually, shear stress distributes uniformly in the shear zone has been suggested by many investigators, such as Hankin et al. [40], Guduru et al. [41], Goyal et al. [42] and so on.

Results from the theory of elasticity show that, the normal stress varies nearly linearly with the distance from the neutral surface [39]. The maxima normal stress is in top and bottom region of the beam, which can be expressed by

$$\sigma = \frac{M}{W} = \frac{\delta q D_{\text{die}}^2}{2DH^2} \tag{4}$$

where W is elastic section modulus of the sample, expressed as $W{=}1/6DH^2$. M is bending couple, which can be given by $M = \frac{1}{12}\delta q D_{\text{die}}^2$. Here, we introduce a parameter δ. This parameter describes the constrained conditions at two ends of the beam, having the value between 0 and 1. $\delta = 0$ corresponding to the simply supported beam, while $\delta = 1$ is the ideal fixed beam. Since tensile stress may promotes the failure of the beam, compressive stress will inhibit the failure. It can be seen that the tensile domain zone at either top or bottom of the shear zone becomes the most dangerous place. Cracks will initiate from these regions. The shear stress, combined with the tensile stress in top or bottom region of the beam, will decide whether the composite has failed and what

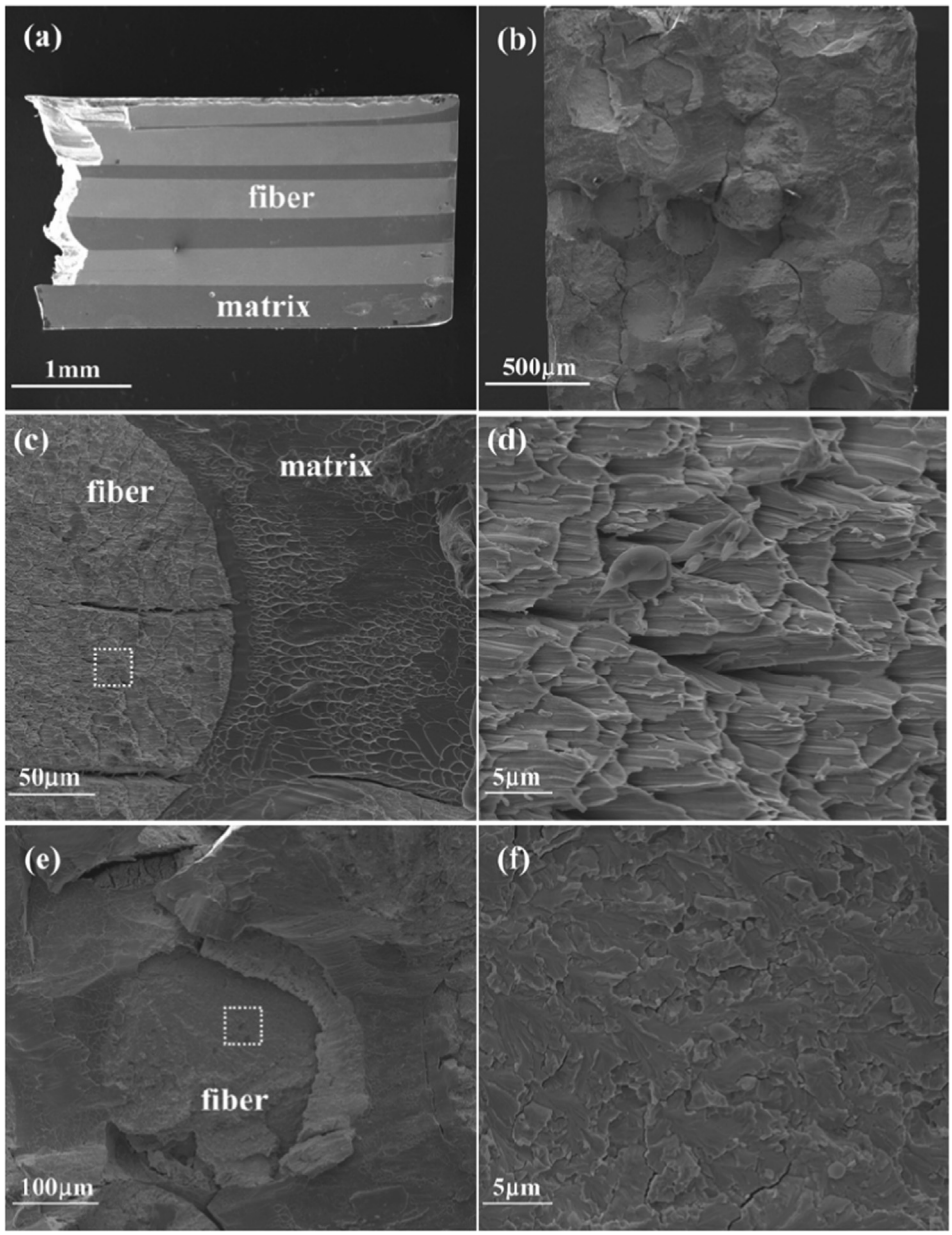

Fig. 6. SEM micrographs showing the fracture feature of composite with 40% V_f (a) Side view of the fractured specimen. (b) Top-view of the fracture surface. (c) Magnification of the fracture surface and (d) Details corresponding to area marked in (c). (e) Another magnified region of (b). (f) Details corresponding to area marked in (e).

failure mode it has. The stress state in the tensile domain zone at either top or bottom of the shear zone is shown in Fig. 9(b).

From Eqs. (3) and (4), τ/σ can be given by

$$\frac{\tau}{\sigma} = \frac{H}{\delta D_{\text{die}}} \tag{5}$$

In the present study, $H = 2.1$ mm, and $D_{die} = 3.5$ mm. Considering the constraint of the cover on the specimen in the shear punch test, 0.8 is chosen for the δ. Then, from Eq. (5), $\tau/\sigma \approx 0.75$. That is to say, the shear stress τ is 0.75 times of the tensile stress σ in the tensile domain zone in the shear zone.

4.2. Failure criterion

The Tsai-Hill failure criterion is commonly used to describe the fracture behaviors of fiber reinforced composites [43-45]. This criterion is expressed as follows

$$\left(\frac{\sigma_1}{X_T}\right)^2 + \left(\frac{\sigma_2}{Y_T}\right)^2 + \left(\frac{\sigma_{12}}{S_{12}}\right)^2 - \left(\frac{\sigma_1}{X_T}\right)\left(\frac{\sigma_2}{Y_T}\right) = 1 \tag{6}$$

Here, σ_1, σ_2 and σ_{12} are in-plane stress components and X_T, Y_T and S_{12} are the normal and in-plane shear strength values. In the present study, as shown in Fig. 9(b), $\sigma_1 = \sigma$, $\sigma_{12} = \tau$ and $\sigma_2 = 0$. The symbols σ_0 and τ_0 are used to replace X_T and S_{12}, respectively. Then, Eq. (6) is simplified as

$$\left(\frac{\sigma}{\sigma_0}\right)^2 + \left(\frac{\tau}{\tau_0}\right)^2 = 1 \tag{7}$$

σ_0 is the longitudinal tensile strength, and τ_0 is the in-plane shear strength.

The Tsai-Hill criterion considers the interaction among the three unidirectional strength parameters of the composite. From this failure criterion, one can determine whether the composite has

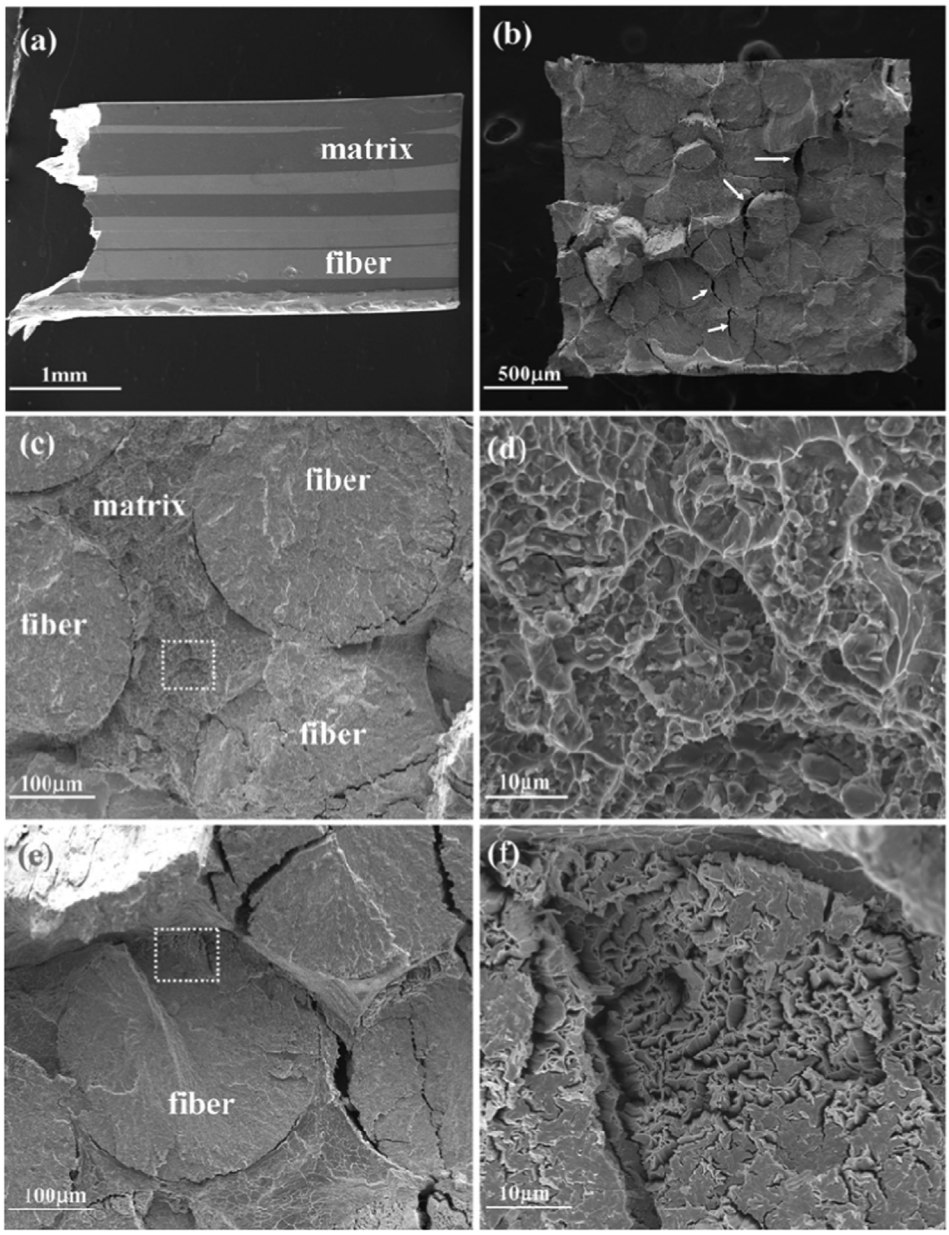

Fig. 7. SEM micrographs showing the fracture feature of composite with 60% V_f (a) Side view of the fractured specimen. (b)–(f) Fracture surface at different magnifications. Arrows in (b) show the micro-crack at the interface area. (d) and (f) are details that corresponding to areas marked in (c) and (e), respectively.

failed. However, the Tsai-Hill criterion does not give the mode of failure. The transition of failure mode with the increasing fiber volume fraction, which is observed in the present shear punch tests of the tungsten fiber/BMG composite, can not be described by this criterion. Therefore, the Tsai-Hill criterion needs to be modified.

Recently, Chen et al. [46] proposed a unified failure criterion for BMGs based on an atomic interaction analysis. In this criterion, the failure modes of BMGs are controlled by the shear-to-normal strength ratio α and the strength-differential factor β. Borrowing the idea from this study, the parameter α is introduced to the Tsai-Hill criterion. Eq. (7) is modified as

$$\left(\frac{\sigma}{\sigma_0}\right)^2 + \left(\frac{\tau}{\alpha\sigma_0}\right)^2 = 1 \tag{8}$$

α is expressed by $\alpha = \tau_0/\sigma_0$, which represents the competition between shear and normal tensile resistance. Geometrically, Eq. (8) constructs the ellipse-like failure envelope in the $\tau - \sigma$ stress space (Fig. 10). The factor α corresponding to the ellipticity of the ellipse. In Fig. 10, the inclined line with the slope of 0.75 represents the stress state on the fracture surface. The point of intersection of the ellipse and the inclined line indicates the fracture point, as marked by "A" in Fig. 10. As shown in Fig. 10(a), with small α, the shear fracture stress τ_f of the fracture point is very close to the shear strength τ_0, while the tensile fracture stress σ_f is much lower than the tensile strength σ_0. This indicates that shear fracture occurs preferentially in the composite. But with large α, τ_f is much lower than τ_0, and σ_f is close to σ_0, as can be seen from Fig. 10(b). Under this condition, tensile fracture is more likely to occur in the composite.

In order to quantitatively describe the failure mode, further discussion is carried out on the modified Tsai-Hill criterion. According to Eqs. (5) and (8), the uniaxial tensile strength σ_0 and pure shear strength τ_0 can be related to the fracture stress σ_f and τ_f, respectively, as expressed by

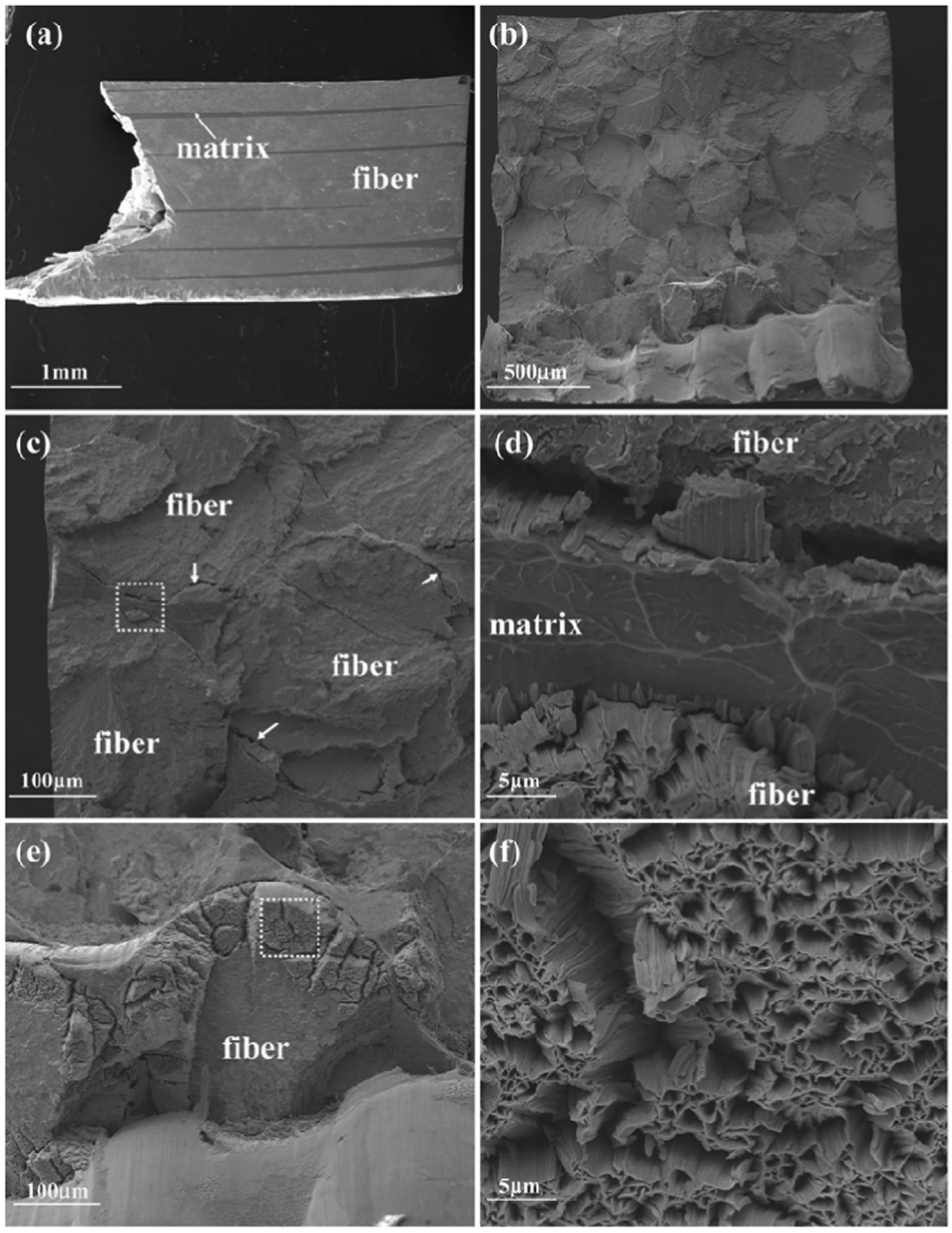

Fig. 8. SEM micrographs showing the fracture feature of composite with 80% V_f (a) Side view of the fractured specimen. (b)–(f) Fracture surface at different magnifications. (d) and (f) are details that corresponding to areas marked in (c) and (e), respectively.

$$\begin{cases} \dfrac{\sigma_f}{\sigma_0} = \sqrt{\dfrac{\alpha^2}{\alpha^2 + 0.75^2}} \\ \dfrac{\tau_f}{\tau_0} = \sqrt{\dfrac{0.75^2}{\alpha^2 + 0.75^2}} \end{cases} \tag{9}$$

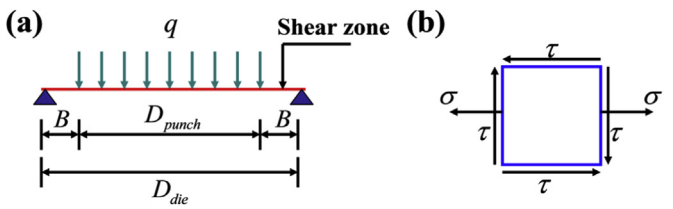

Fig. 9. (a) Simplification of the shear punch test. (b) Stress state in the shear zone.

Fig. 11 shows the variations of the normalized strength in Eq. (9) with α. As shown in this plot, τ_f/τ_0 decreases and σ_f/σ_0 increases respectively with α increasing. These two lines intersect at $\alpha = 0.75$. For $\alpha < 0.75$, τ_f/τ_0 is higher than σ_f/σ_0. In this case, the difference between σ_f and σ_0 is more significant than the difference between τ_f and τ_0. In other words, on the fracture plane, τ_f is close to τ_0, while σ_f is much lower than σ_0. Shearing will dominate the failure of the composite. But for $\alpha > 0.75$, σ_f/σ_0 becomes higher. This indicates that σ_f is close to σ_0 on the fracture surface. Tensile fracture becomes the dominant failure mode in this case. It can conclude that $\alpha = 0.75$ is the critical value for shear-tensile fracture transition.

4.3. Transition of failure mode

From the discussion in Section 4.2, it can be seen that the failure mode is dependent on shear-to-normal strength ratio α. The

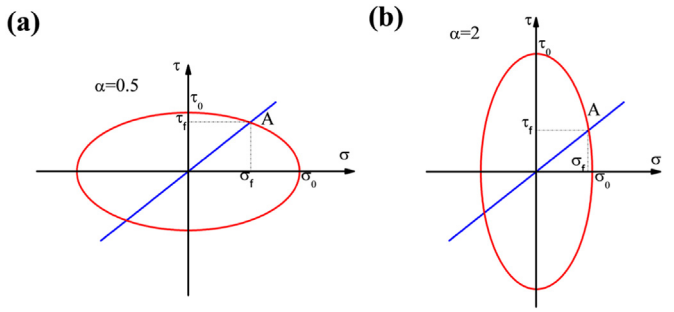

Fig. 10. Ellipse-like failure envelope in $\tau - \sigma$ stress space. The point marked "A" represents the fracture point. (a) The shear-to-tensile factor $\alpha = 0.5$ and (b) $\alpha = 2$.

micromechanical analysis of the variation of shear-to-normal strength ratio α with tungsten fiber volume fraction will be made in this section.

Table 1 gives the properties of the Vit1 BMG and tungsten fiber. Supposing the tensile strength of tungsten fiber/BMG composite obeys the rule of mixtures. Then σ_0 is expressed as

$$\sigma_0 = \sigma_w V_f + \sigma_m\left(1 - V_f\right) \tag{10}$$

where σ_w is tensile strength of the tungsten fiber, which has the value of 2.35 *GPa* [18,19,24,25]. σ_m is the normal (ideal) tensile strength of Vit1 BMG matrix. According to the study by Chen et al. [46], the shear-to-normal strength ratio α has the value of 0.33 for this BMG, i.e., $\alpha = \tau_m/\sigma_m = 0.33$. The shear strength τ_m of Vit1 BMG is about 1.10 GPa [30,47]. Thus, $\sigma_m = 3.33$ *GPa* is obtained for the BMG matrix.

Under shearing stress loading, one can assume that the composite behaves elastically. This can be evidenced by the stress–-strain curves (Fig. 3). Furthermore, under shear loading, the interface between the tungsten fiber and Vit1 BMG is well bonded, which can be seen from the shear fracture plane of the composite with 40% V_f (Fig. 6(c)). Then, it is reasonable to presume that the tungsten fiber and Vit1 BMG have the same shear displacement. As a result, the shear strains in the fiber and the matrix are equal. Then, the in-plane shear strength can be given by

$$\tau_0 = G_{12}\gamma_m \tag{11}$$

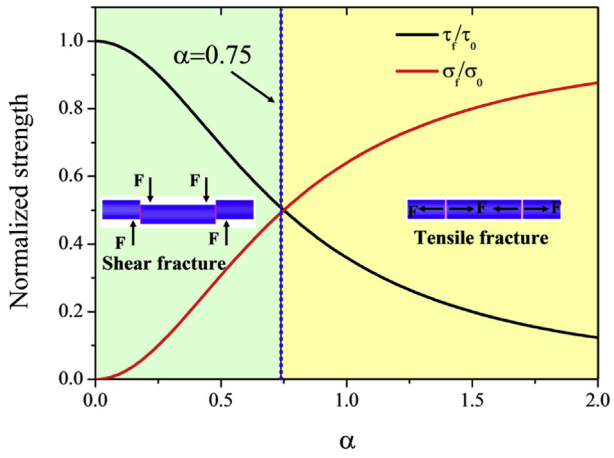

Fig. 11. Dependent of normalized strength τ_f/τ_0 and σ_f/σ_0 on α.

Table 1
Physical properties of Vit1 BMG and tungsten fiber.

Properties	Vit1 BMG	Tungsten fiber
Young's modulus (GPa)	96	410
Shear modulus (GPa)	34.3	160.5
Normal tensile strength (GPa)	3.33	2.35
Shear strength (GPa)	1.1	–
Shear fracture strain (%)	3.2	–

γ_m is the shear fracture strain of the BMG matrix, which has the value of 0.032. G_{12} is the in-plane shear modulus of the composite, as can be expressed by Ref. [48]

$$G_{12} = G_m\left[\frac{G_f\left(1+V_f\right)+G_m\left(1+V_f\right)}{G_f\left(1-V_f\right)+G_m\left(1+V_f\right)}\right] \tag{12}$$

where G_f and G_m are the shear modulus of the tungsten fiber and BMG matrix, respectively.

Using the values of the parameters given in Table 1, the shear strength and tensile strength of the composite as a function of the fiber volume fraction are plotted in Fig. 12(a). From this figure, it can be seen that the tensile strength decreases gradually with the increasing fiber volume fraction. This tendency is consistent with the experimental results of Conner et al. [18]. and Qiu et al. [19]. However, with the fiber volume fraction increasing, the shear strength increases. The functional dependence of the shear-to-normal strength ratio $\alpha = \tau_0/\sigma_0$ on the fiber volume fraction is presented in Fig. 12(b). As shown in this figure, with the fiber volume fraction increasing from 0% to 80%, α increases from 0.33 to 1.36. For composite with 0% V_f (Vit1 BMG matrix), $\alpha = 0.33$, which is lower than 0.75. According to the modified Tsai-Hill criterion discussed in Section 4.2, shearing will act as the dominant failure mode for this material. $\alpha = 0.64$ is obtained for composite with 40% V_f. This value is close to 0.75. The mixed failure mode, with shear and tensile fracture, may occur in this material. But the dominant failure mode is the shear fracture. For composite with 60% and 80% V_f, 0.91 and 1.36 are obtained for the α, respectively. Both of the values are higher than 0.75. Then, these two materials will fail by tensile fracture. These results are consistent with the phenomenon observed for the tested materials in the present shear punch test, as shown in Section 3.2.

4.4. Underlying mechanisms of failure

From the above analysis, the transition of failure mode is illustrated quite well by the modified Tsai-Hill criterion. In this section, the possible mechanisms of failure will be discussed.

According to the previous study [32], tungsten fiber demonstrates necking under uniaxial tension. However, lateral deformation is hardly observed for the Vit1 BMG loaded by tension [27,31]. The differences in lateral deformation between these two phases can result in radial tensile stress at the fiber/matrix interface. Once this radial tensile stress overcomes the bonding strength, debonding will occur at the interface. This is the reason for the existence of micro-crack at the fiber/matrix interface on the tensile fracture plane, as shown in Figs. 7(b) and Fig. 8(c). In this case, the interface will act as the weak region, which reduces the resistance to tensile fracture of the composite. For composite with high fiber volume fraction, the interface takes a relative high volume fraction, resulting in lower tensile strength. This illustrates that why the tensile strength decreases with the increasing fiber volume fraction, as shown in Fig. 12(a).

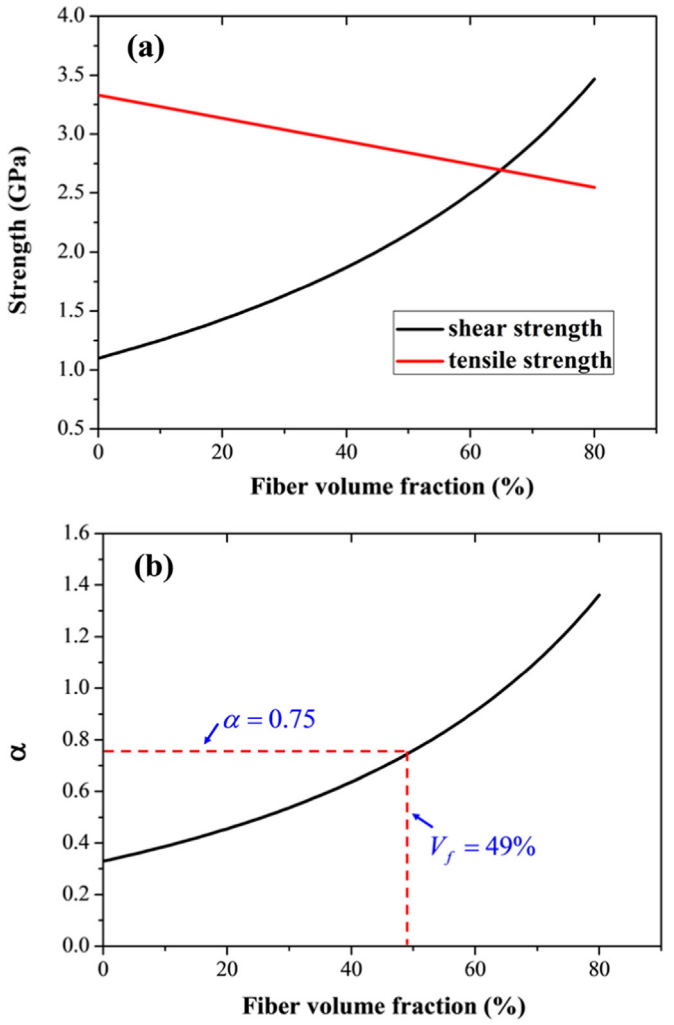

Fig. 12. (a) Uniaxial tensile strength σ_0 and pure in-plane shear strength τ_0 vary with the tungsten fiber volume fraction. (b) Dependent of α on the tungsten fiber volume fraction.

As shown in Fig. 12(a), increasing fiber volume fraction increases the shear strength of the composite. Because of deformation compatibility between the tungsten fiber and Vit1 BMG, the interface is well bonded. This can be seen from the shear fracture surface of composite with 40% V_f (Fig. 6(c)). Furthermore, shear strength of 1.51 GPa of bulk tungsten was given by Grady [49]. Supposing the tungsten fiber obeys the Von-Mises criterion. Since limited data of shear property of single as-drawn tungsten fiber can be found, it is reasonable to presume that the shear strength of tungsten fiber is 3/3 of the tensile strength (2.35 GPa), i.e., shear strength is about 1.36 GPa. This strength is higher than the Vit1 BMG (1.10 GPa). Tungsten fiber will serve as the reinforcing phase for the composite. Then, with the increasing fiber volume fraction, shear strength of the composite increases.

The ratio $\alpha = \tau_0/\sigma_0$, i.e., fracture mode factor, reflects the competition between shear deformation and normal fracture. α increases with the increasing fiber volume fraction. $\alpha = 0.75$ is the critical value for shear-tensile fracture transition. For $\alpha < 0.75$, the shear strength is small while the tensile strength is large. In this case, the composite is much easy to behave in shear deformation and the tensile stress acting on the fracture surface only plays a weak role. Furthermore, $\alpha < 0.75$ corresponding to $V_f < 49\%$, as can be seen from Fig. 12(b). For composite with low fiber volume fraction, the Vit1 BMG matrix would control the deformation of the composite, i.e., shearing occurs preferentially for the composite. While in the $V_f > 49\%$ case, $\alpha > 0.75$ is obtained. For composite with high fiber volume fraction, the effect of Vit1 BMG matrix becomes weak. The fracture of composite is dominated by the tungsten fiber or the fiber/matrix interface. $\alpha > 0.75$ indicates that the tensile strength of the composite is small and becomes the controlling factor for the failure of composite, which means that the composite is easy to fail in the tensile fracture mode but hard to display shear deformation.

5. Conclusions

In this study, transverse dynamic shear punch tests were carried out on the tungsten fiber/Vit1 BMG composite. The failure mode of this composite is found to change from shear fracture to tensile fracture with increasing the fiber volume fraction. A modified Tsai-Hill criterion, in which the shear-to-normal factor α is considered, is proposed to characterize the different fracture behaviors of the composite. It is found that $\alpha = 0.75$ is the critical value for shear-tensile fracture transition. The functional dependence of α on the fiber volume fraction is derived by micromechanical analysis. The composite with fiber volume fraction lower than 49% is corresponding to $\alpha < 0.75$. In this case, the shear strength is small while the tensile strength is large. Shearing acts as the dominant failure mode. In the case of fiber volume fraction is higher than 49%, which corresponding to $\alpha > 0.75$, the tensile strength becomes the controlling factor for composite failure.

Acknowledgments

Financial support is from the National Natural Science Foundation of China (Grants Nos. 11132011, 11202221, 11372315), the National Natural Science Foundation of China-NSAF Grant No: 10976100 and the National Key Basic Research Program of China (Grant No. 2012CB937500). Research supported by the CAS/SAFEA International Partnership Program for Creative Research Teams.

References

[1] Trexler MM, Thadhani NN. Mechanical properties of bulk metallic glasses. Prog Mater Sci 2010;55:759–839.
[2] Greer AL, Ma E. Bulk metallic glasses: at the cutting edge of the metals research. MRS Bull 2007;32:611–9.
[3] Schuh CA, Hufnagel TC, Ramamurty U. Mechanical behavior of amorphous alloys. Acta Mater 2007;55:4067–109.
[4] Wang WH. The elastic properties, elastic models and elastic perspectives of metallic glasses. Prog Mater Sci 2012;57:487–656.
[5] Dai LH, Yan M, Liu LF, Bai YL. Adiabatic shear banding instability in bulk metallic glasses. Appl Phys Lett 2005;87:141916.
[6] Dai LH, Bai YL. Basic mechanical behaviors and mechanics of shear banding in BMGs. Int J Impact Eng 2008;35:704–16.
[7] Jiang MQ, Dai LH. On the origin of shear banding instability in metallic glasses. J Mech Phys Solids 2009;57:1267–92.
[8] Miracle DB, Concustell A, Zhang Y, Yavari AR, Greer AL. Shear bands in metallic glasses: size effects on thermal profiles. Acta Mater 2011;59:2831–40.
[9] Dodd B, Bai YL, editors. Adiabatic shear localization. 2nd ed. London: Elsevier; 2012. pp. 311–61.
[10] Greer AL, Cheng YQ, Ma E. Shear bands in metallic glasses. Mater Sci Eng R 2013;74:71–132.
[11] Chen Y, Jiang MQ, Dai LH. Collective evolution dynamics of multiple shear bands in bulk metallic glasses. Int J Plasticity 2013;50:18–36.
[12] Yim HC, Conner RD, Szues F, Johnson WL. Processing, microstructure and properties of ductile metal particulate reinforced $Zr_{57}Nb_5Al_{10}Cu_{15.4}Ni_{12.6}$ bulk metallic glass composites. Acta Mater 2002;50:2737–45.
[13] Hofmann DC, Suh JY, Wiest A, Duan G, Lind ML, Demetriou MD, et al. Designing metallic glass matrix composites with high toughness and tensile ductility. Nature 2008;451:1085–9.
[14] Martin M, Meyer L, Kecskes L, Thadhani NN. Uniaxial and biaxial compressive response of a bulk metallic composite over a range of strain rates and temperatures. J Mater Res 2009;24:66–78.

[15] Wu Y, Zhou DQ, Song WL, Wang H, Zhang ZY, Ma D, et al. Ductilizing bulk metallic glass composite by tailoring stacking fault energy. Phys Rev Lett 2012;109:245506.
[16] Chen JH, Jiang MQ, Chen Y, Dai LH. Strain rate dependent shear banding behavior of a Zr-based bulk metallic glass composite. Mater Sci Eng A 2013;576:134–9.
[17] Dandliker RB, Conner RD, Johnson WL. Melt infiltration casting of bulk metallic-glass matrix composites. J Mater Res 1998;13:2896–901.
[18] Conner RD, Dandliker RB, Johnson WL. Mechanical properties of tungsten and steel fiber reinforced $Zr_{41.25}Ti_{13.75}Cu_{12.5}Ni_{10}Be_{22.5}$ metallic glass matrix composites. Acta Mater 1998;46:6089–102.
[19] Qiu KQ, Wang AM, Zhang HF, Ding BZ, Hu ZQ. Mechanical properties of tungsten fiber reinforced ZrAlNiCuSi metallic matrix composite. Intermetallics 2002;10:1283–8.
[20] Hou B, Li YL, Xing LQ, Chen CS, Kou HC, Li JS. Dynamic and quasi-static mechanical properties of fiber-reinforced metallic glass at different temperatures. Philos Mag Lett 2007;87:595–601.
[21] Chen XW, Chen G. Experimental research on the penetration of tungsten-fiber/metallic-glass matrix composite material penetrator into steel target. EPJ Web Conf 2012;26:01049.
[22] Conner RD, Dandliker RB, Scruggs V, Johnson WL. Dynamic deformation behavior of tungsten-fiber/metallic-glass matrix composites. Int J Impact Eng 2000;24:435–44.
[23] Yim HC, Conner RD, Szuecs F, Johnson WL. Quasistatic and dynamic deformation of tungsten reinforced $Zr_{57}Nb_5Al_{10}Cu_{15.4}Ni_{12.6}$ bulk metallic glass matrix composites. Scr Mater 2001;45:1039–45.
[24] Zhang H, Zhang ZF, Wang ZG, Qiu KQ, Zhang HF, Zang QS. Effects of tungsten fiber on failure mode of Zr-based bulk metallic glassy composite. Metall Mater Trans A 2006;37:2459–69.
[25] Wang H, Zhang HF, Hu ZQ. Tungsten fiber reinforced Zr-based bulk metallic glass composites. Mater Manuf Process 2007;22:687–91.
[26] Grady DE. Properties of an adiabatic shear-band process zone. J Mech Phys Solids 1992;40:1197–215.
[27] Jiang MQ, Dai LH. Shear-band toughness of bulk metallic glasses. Acta Mater 2011;59:4525–37.
[28] Dai LH, Bai YL. Transverse shear strength of unidirectional carbon fiber reinforced aluminum matrix composite under static and dynamic loadings. J Compos Mater 1998;32:246–57.
[29] Li YL, Guo YZ, Hu HT, Wei Q. A critical assessment of high-temperature dynamic mechanical testing of metals. Int J Impact Eng 2009;36:177–84.
[30] Liu LF, Dai LH, Bai YL, Wei BC. Initiation and propagation of shear bands in Zr-based bulk metallic glass under quasi-static and dynamic shear loadings. J Non-Crystalline Solids 2005;351:3259–70.
[31] Jiang MQ, Ling Z, Meng JX, Dai LH. Energy dissipation in fracture of bulk metallic glass via inherent competition between local softening and quasi-cleavage. Philos Mag 2008;88:407–26.
[32] Leber S, Tavernelli J, White DD. Fracture modes in tungsten wire. J Less-Common Metals 1976;48:119–33.
[33] Gilbert CJ, Schroeder V, Ritchie RO. Mechanisms for fracture and fatigue-crack propagation in a bulk metallic glass. Metall Mater Trans A 1999;30:1739–53.
[34] Escobedo JP, Gupta YM. Dynamic tensile response of Zr-based bulk amorphous alloys: fracture morphologies and mechanisms. J Appl Phys 2010;107:123502.
[35] Jiang MQ, Meng JX, Keryvin V, Dai LH. Crack branching instability and directional stability in dynamic fracture of a tough bulk metallic glass. Intermetallics 2011;19:1775–9.
[36] Raghavan R, Murali P, Ramamurty U. On factors influencing the ductile-to-brittle transition in a bulk metallic glass. Acta Mater 2009;57:3332–40.
[37] Li QM, Jones N. Formation of shear localization in structural elements under transverse dynamic loads. Int J Solids Structures 2000;37:6683–704.
[38] Li QM, Jones N. Response and failure of a double-shear beam subjected to mass impact. Int J Solids Structures 2002;39:1919–47.
[39] Timoshenko SP, Goodier JN. Theory of elasticity. 3rd ed. New York: McGraw-Hill; 1970. pp. 41–50.
[40] Hankin GL, Toloczko MB, Jhoson KI, Khaleel MA, Hamilton ML, Garner FA, et al. An investigation into the origin and nature of the slope and x-axis intercept of the shear punch-tensile yield strength correlation using finite element analysis. ASTM STP 2000;1366:1018–28.
[41] Guduru RK, Nagasekhar AV, Scattergood RO, Koch CC, Murty KL. Finite element analysis of a shear punch test. Metall Mater Trans A 2006;37:1477–83.
[42] Goyal Sunil, Karthik V, Kasiviswanathan KV, Valsan M, Bhanu Sankara Rao K, Baldev Raj. Finite element analysis of shear punch testing and experimental validation. Mater Des 2010;31:2546–52.
[43] Arola D, Ramulu M. Orthogonal cutting of fiber-reinforced composites: a finite element analysis. Int J Mech Sci 1997;39:597–613.
[44] Naik NK, Chandra Sekher Y, Meduri Sailendra. Damage in woven-fabric composites subjected to low-velocity impact. Compos Sci Technol 2000;60:731–44.
[45] John RM. Mechanics of composites. Washington (DC): Scripta Book Company; 1975.
[46] Chen Y, Jiang MQ, Wei YJ, Dai LH. Failure criterion for metallic glasses. Philos Mag 2011;91:4536–54.
[47] Lu J, Ravichandran G, Johnson WL. Deformation behavior of the $Zr_{41.2}Ti_{13.8}Cu_{12.5}Ni_{20}Be_{22.5}$ bulk metallic glass over a wide range of strain-rate and temperatures. Acta Mater 2003;51:3429–43.
[48] Kaw AK. Mechanics of composite materials. 2nd ed. London: Talor and Francis; 2006. pp. 256–68.
[49] Grady DE. Dissipation in adiabatic shear bands. Mech Mater 1994;17:289–93.